In situ mass spectrometry imaging reveals metabolite alterations in gray and white matter after spinal cord injury

CHENGHAO LYU[1], YUJING TANG[1,2] and FEI-FEI SHANG[1]

[1]International Medical College and College of Basic Medicine, Chongqing Medical University, Chongqing 400016, P.R. China; [2]College of Medical Laboratory Science and Technology, Harbin Medical University, Daqing, Heilongjiang 163319, P.R. China

Received November 4, 2024; Accepted March 19, 2025

DOI: 10.3892/etm.2025.12867

Abstract. It is known that spinal cord injury (SCI) causes metabolic disorders, such as disrupted lipid and amino acid metabolism. However, the *in situ* changes of metabolites in the spinal cord remain elusive. In the present study, adult Sprague-Dawley rats underwent spinal cord transection surgery. Ambient air flow-assisted desorption electrospray ionization mass spectrometry imaging was performed to identify the localization of metabolites in the white and gray matter and the ventral and dorsal horns within the spinal cord sections. The results revealed that 42 metabolites were specifically increased in the gray matter, and 90 metabolites were increased in the white matter compared with that in the sham group. In the ventral and dorsal horns, 86 and 103 metabolites, respectively, exhibited specific increases after injury. By contrast, numerous metabolites, especially lipids, were significantly decreased after SCI. Phosphatidylserine and phosphatidylethanolamine were mainly decreased in the gray matter, while cholesterol and ceramide were mainly decreased in the white matter. Specifically, phosphatidylethanolamine was detected at low levels in the dorsal horn following injury. However, the phosphatidylserine level decreased in the ventral horn. The functional enrichment of these metabolites via Kyoto Encyclopedia of Genes and Genomes analysis further confirmed the profile differences in the white and gray matter, as well as in the ventral and dorsal horns after SCI. These results provide valuable information on the metabolite profiles across various anatomical regions of the spinal cord following SCI, which may support the development of precise treatment strategies for patients.

Correspondence to: Professor Fei-Fei Shang, International Medical College and College of Basic Medicine, Chongqing Medical University, 1 Yixueyuan Road, Yuzhong, Chongqing 400016, P.R. China
E-mail: sff_phoenix@cqmu.edu.cn

Key words: spinal cord injury, spatial metabolomics, gray matter, white matter

Introduction

The spinal cord is an important part of the central nervous system that connects the brain and peripheral nerves. Spinal cord injury (SCI) is caused directly or indirectly by various factors, including sports injuries, traffic accidents, tumors, infections and toxins. The number of annual new cases of SCI has reached 500,000 worldwide (1). SCI is usually divided into two stages according to the chronological order of damage: Primary and secondary. Primary injury occurs unexpectedly and refers to the initial traumatic injury. Secondary injury occurs as a consequence of the changes induced by a primary injury, such as inflammation, fibrotic scar formation and oxidative stress (2-4).

In cross-sections, the peripheral region of the spinal cord contains neuronal white matter tracts. The gray matter, which is mainly composed of neuron bodies, is internal to the white matter. The gray matter is butterfly-shaped, with the four 'wings' called horns. The two ventral horns contain motor neurons while the two dorsal horns contain sensory neurons (5,6). Previous studies on SCI have only discussed metabolite changes in the spinal cord as a whole (7,8). As the spinal cord is composed of the aforementioned different physiological structures, we hypothesized that metabolite changes may differ in these structures after injury.

Metabolites are small molecules produced by metabolic reactions catalyzed by various enzymes, such as aldolase and phosphofructokinase in glucose metabolism. They are fundamental components of organisms and cells, providing energy and transmitting signals (9) In previous years, various metabolites that change after SCI have been detected (10). For example, catecholamines and norepinephrine accumulate in the spinal cord, causing vasospasm and accelerating inflammatory storms. The release of aspartate and glutamate following SCI has been observed to induce neurotoxicity, while retinoic acid has a neuroprotective effect (7,8). However, the aforementioned studies have not provided information about the chemical and metabolic processes involved in the different anatomical structures of the spinal cord.

Spatial metabolomics is a rapidly emerging field fueled by the development of mass spectrometry imaging and hyperspectral imaging data analysis. The technique can characterize biological phenomena *in situ* and detect changes in metabolites, lipids and drugs in tissue sections (11). The present study

employed spatial metabolomics to explore SCI-induced metabolite changes in different regions, including the white and gray matter, and the ventral and dorsal horns. This analysis offers precise characterization of the metabolite profiles across various anatomical regions of the spinal cord following SCI.

Materials and methods

Animal model preparation. The animal experiments in the current study were approved by the Chongqing Medical University Ethics Committee on Animal Research (Chongqing, China; approval no. 2022-0115). Following the Resource Equation Approach formula, the sample size for each group was set at 6 (12). A total of 12 adult female Sprague-Dawley rats (6-7 weeks old, weighing 180-220 g) were obtained from the Experimental Animal Center of Chongqing Medical University, China. The rats were housed under standard conditions at room temperature with a 12-h light/dark cycle and had free access to food and water. Anesthesia was induced with 3% isoflurane and maintained at a concentration of 2%. Approximately 1 cm of the T10 spinal cord was exposed in both groups. In the sham group (n=6), the spinal cord was left untreated. In the SCI group (n=6), ophthalmic scissors were used to transect the spinal cord, and ~2 mm of tissue from the center of the exposed area was removed. A needle was passed back and forth through the gap several times to ensure complete severance of the nerve before the wound was sutured. The animals underwent daily bladder expression for urination until euthanasia. The Basso, Beattie and Bresnahan (BBB) locomotor rating scale was used on the third postoperative day to confirm the complete loss of hind limb function (Fig. S1A) (13). The health and welfare of the rats were regularly monitored. Humane endpoints included weight loss >20%, persistent refusal to eat or drink for >24 h and signs of respiratory distress, such as labored breathing, wheezing or cyanosis. However, none of the rats died or reached the defined humane endpoints. After 7 days, the animals were euthanized by cervical dislocation following anesthesia with 2% pentobarbital sodium (200 mg/kg), administered via intraperitoneal injection. Death was verified by the cessation of circulatory and respiratory functions, along with the loss of reflexes. The spinal cord was removed, and the rostral spinal cord was quickly stored at -80˚C until further use.

Mass spectrometry imaging (MSI). The primary injury stage, occurring 0-14 days after SCI, is also considered the acute phase (2-4). Therefore, in the present study, the seventh day post-injury was selected to detect metabolite changes induced by traumatic injury. The tissue samples were sectioned (15 μm) at -20˚C by a Leica CM1950 cryostat. After fixation in 4% paraformaldehyde at room temperature for 30 sec, one section was subjected to H&E staining. Hematoxylin staining was performed at room temperature for 5 min, followed by eosin counterstaining for 1 min. The stained section was then examined using a bright-field microscope (Leica, Inc.). The MSI data were acquired via an air flow-assisted ionization-MSI platform [Victor (Beijing) Technology Co., Ltd.] and a Q Exactive Orbitrap mass spectrometer (Thermo Fisher Scientific, Inc.). Mass spectrometry data acquisition was performed in progressive scanning mode. The experimental platform parameters were set as follows: Capillary temperature at 350˚C, scan range from 70 to 1,000 Da, spray gas pressure at 0.6 MPa, spray angle at 60˚, extraction gas flow at 45 l/min, X-axis scan speed of 0.16 mm/sec, Y-axis step spacing of 0.04 mm, and a delay time of 7 sec. The scanning length for both the X-axis and Y-axis was 10 mm. Data acquisition was performed via Xcalibur 4.2 software (Thermo Fisher Scientific, Inc.), which recorded the spatial location and intensity of all the detected ions. Both positive and negative ion modes were used for MSI analysis. For the positive ion scanning mode, the spray solvent composition was acetonitrile:water=80:20 (v/v), containing 0.1% formic acid. For the negative ion scanning mode, the solvent composition was acetonitrile:water=80:20 (v/v) without formic acid. The flow rate of the spray solvent was 5 μl/min.

MSI data analysis. The raw mass spectrometry data were further processed through data filtering, compression, dimensionality reduction, feature extraction and image reconstruction using an R package (Cardinal MSI; version 3.0) (14). To visualize the results of clustering the overall expression levels, cluster analysis was performed using spatially shrunken centroid clustering (k-means) to identify different regions within the tissue. The Pearson correlation coefficient was used to measure the degree of linear correlation between two clusters. The correlations were computed based on the ion intensities detected within each cluster, and the Bonferroni correction was applied to control the family-wise error rate across all Pearson correlation analyses. The orthogonal partial least squares-discriminant analysis (OPLS-DA) approach and permutation test was used to discriminate between the two groups (SIMCA 14.1 Umetrics). Next, a comparative analysis was conducted to identify the differentially expressed mass-to-charge (m/z) signals between different regions of interest in the tissue sections. In addition, the variable importance in projection (VIP) values and fold changes (FCs) were calculated, and a Student's t-test was conducted to compare the significance of m/z signals between groups. The VIP values, P-values and FCs were visualized using volcano plots, which facilitated the identification of differential m/z signals. The signals with VIP values >1 and P-values <0.05 were considered to exhibit significant and reliable changes. An in-house SmetDB database (Shanghai Luming Biotechnology Co., Ltd.) was used to annotate the m/z signal data and identify the altered metabolites. Functional enrichment of differential metabolites was performed using the Kyoto Encyclopedia of Genes and Genomes database (https://www.kegg.jp/). The hypergeometric test was used to identify significantly enriched terms (P<0.05), and the results are displayed using bubble charts.

Quantitative analysis of metabolites. Spinal cord samples were homogenized in 4.5 ml $CHCl_3$/MeOH (2:1, v/v) and centrifuged at 10,000 x g for 5 min at 4˚C to remove debris. The supernatant was then mixed with 1.25 ml distilled H_2O to induce phase separation. The lower (chloroform) organic phase was collected, and the upper phase was mixed with 2 ml $CHCl_3$/MeOH/H_2O (86:14:1, v/v/v) to perform a second extraction. The organic phases from both extractions were combined and subsequently dried in a vacuum centrifuge at 200 x g and 15˚C for 60 min. The resulting residue was then

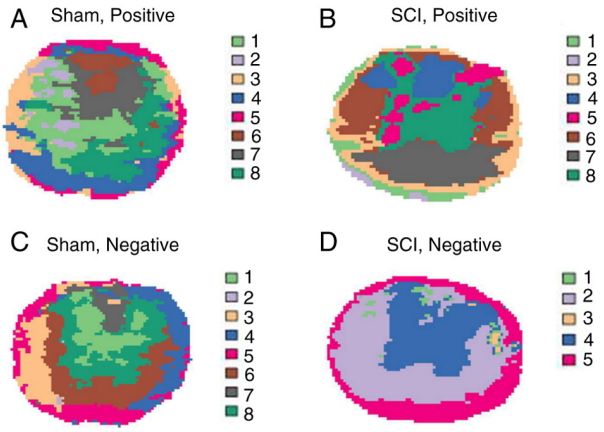

Figure 1. Metabolite profiles are different in various regions of the spinal cord. (A) Spatial shrunken centroids clustering analysis (k-means) of sham group under positive mode. (B) Clustering analysis of SCI group under positive mode. (C) Clustering analysis of sham group under negative mode. (D) Clustering analysis of SCI group under negative mode Different clusters are displayed in distinct colors and labeled numerically. Regions with the same color have more similar metabolite profiles. 'Positive' refers to positive ion mode of the mass spectrum, while 'negative' refers to negative ion mode. SCI, spinal cord injury.

dissolved in 200 μl $CHCl_3$/MeOH/H_2O (60:30:4.5, v/v/v). The following ELISA kits were used to detect metabolite contents according to the manufacturers' protocols: Phosphatidylserine (PS; cat. no. EKU08732; Biomatik), phosphatidylethanolamine (PE; cat. no. MAK361; MilliporeSigma), cholesterol (CE; cat. no. CS0005; MilliporeSigma), ceramide (Cer; cat. no. A326471; Antibodies) and phosphatidic acid (PA; cat. no. MET-5019; Cell Biolab). The concentration of each metabolite in the samples was calculated using a standard curve. The data were normalized to the mean value of the sham group.

Statistical analysis. GraphPad 9.5 software (Dotmatics) was used for statistical analysis. The data are presented as the mean ± standard deviation. Unpaired Student's t-test was used for comparisons between two groups, while the BBB score was analyzed using the non-parametric Mann-Whitney U test. $P<0.05$ was considered to indicate a statistically significant difference.

Results

Different anatomical structures of spinal cord exhibit various metabolite profiles after SCI. Contiguous spinal cord sections with intact morphology (without any breaks or crushing) were selected for MSI analysis in both positive and negative modes (Fig. S1B). The data were then subjected to unsupervised clustering analysis, specifically, spatially shrunken centroid clustering analysis, as shown in Fig. 1. These clusters largely corresponded to the different structures of the spinal cord in the two-dimensional plane. This indicated that the metabolites in different regions of the spinal cord may exhibit certain specificity, especially after SCI. For example, in the negative mode, cluster 4 was highly matched with the gray matter, whereas clusters 2 and 5 were predominantly located in the white matter.

Correlation analysis of these clusters revealed strong positive correlations between clusters located in the same morphological structure (Fig. S1C). For instance, in the SCI group under the positive mode, clusters 6 and 7, located in the white matter, exhibited strong positive correlations, similar to clusters 5 and 8 in the gray matter. Conversely, the clusters located in different structures displayed strong negative correlations, such as clusters 3 and 8 in the SCI group under the positive mode. Therefore, it is necessary to separately analyze the metabolic changes in different structures of the spinal cord to obtain more detailed and accurate results.

Differential changes in gray and white matter metabolites after SCI. Mass spectrometry results showed that a total of 3,077 m/z signals were collected, including 255 signals in the negative mode and 2,822 signals in the positive mode. Based on the coordinates, mass spectrometry data for the white and gray matter were separated and subjected to multivariate statistical analysis (OPLS-DA) to distinguish the overall differences in metabolic profiles between the groups (Fig. 2A). To prevent model overfitting, seven-fold cross-validation and 200 response permutation tests were used to assess the validity of the model (Fig. S2). The reliability of the OPLS-DA model was assessed using the R^2Y and Q^2Y parameters. If the R^2Y and Q^2Y values are close to 1 (the slopes of the R^2 and Q^2 lines are closer to 45°), the models have high goodness-of-fit and predictive abilities. The results showed that all these values were >0.5. For example, in the gray matter, under positive ion mode, $R^2Y=0.982$ and $Q^2Y=0.965$; under negative ion mode, $R^2Y=0.854$ and $Q^2Y=0.814$. These data indicate that the OPLS-DA results are reliable (15). Additionally, the VIP values were calculated. Higher VIP values indicated a greater contribution of the variable to group separation. In the present study, m/z signals with VIP values >1 were further analyzed for differential metabolites.

Subsequently, the P-values and FCs for each m/z signal after SCI were calculated. A total of 104 signals VIP values >1 with $P<0.05$ were identified in the gray matter. Of these, 85 were in the positive mode, with 64 metabolites elevated and 21 decreased, while 19 were in the negative mode, with 18 elevated and 1 decreased in the SCI model compared with those in the sham group. A total of 140 signals VIP values >1 with $P<0.05$ were identified in the white matter. Of these, 123 were in the positive mode, with 97 elevated and 26 decreased, while all 17 signals in negative mode were elevated, with none showing a decrease under SCI conditions. (Fig. 2B). These mass spectrometry data were further annotated to metabolites via the SmetDB database. The results revealed 315 differential metabolites in the gray matter and 404 differential metabolites in the white matter (Table SI). Comparative analysis of these differential metabolites showed that 205 metabolites were increased in both the gray and white matter, whereas 32 metabolites were decreased in both the gray and white matter. Overall, a large number of metabolites were elevated in the SCI group. And a substantial portion of the decreased metabolites were lipid. For instance, PS, PE and PGP mainly decreased in the gray matter, CE and Cer mainly decreased in the white matter, and PA decreased in both the gray and white matter (Table SII). The raw m/z signal heatmaps for these representative metabolites were also displayed in Fig. 3.

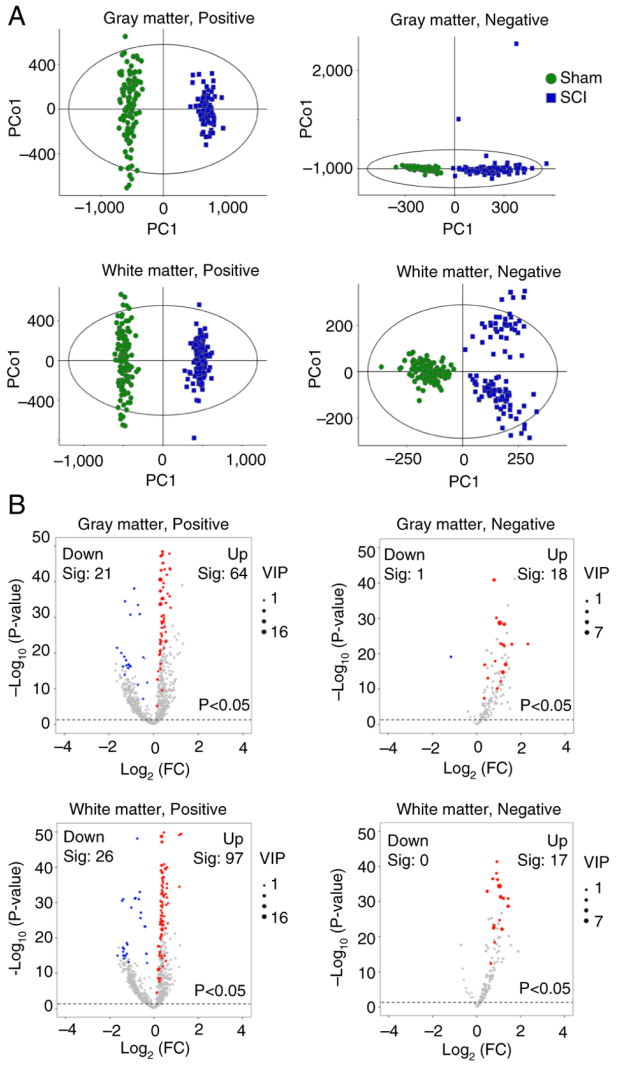

Figure 2. Analysis of metabolite changes in gray and white matter following SCI. (A) Group separation on orthogonal partial least squares-discriminant analysis score plots. (B) Mass-to-charge ratio signals showing content changes are displayed by volcano plots. The horizontal dotted lines show the cut-off level of P<0.05. Signals with VIP values >1 are colored. Red dots represent upregulation, and blue dots represent downregulation. FC, fold change; VIP, variable importance in projection; SCI, spinal cord injury; PC1, principal component 1; PoC1, first orthogonal component; Sig, significant.

Differential changes in metabolites in the ventral horn and dorsal horn. The mass spectrometry data of the ventral and dorsal horns of the gray matter were further separated based on the coordinates, and OPLS-DA was performed to distinguish the overall metabolic profile differences between the groups (Fig. 4A). The reliability of the OPLS-DA model was assessed using the R^2Y and Q^2Y parameters, such as in the ventral horn, under positive ion mode, R^2Y=0.99 and Q^2Y=0.971; under negative ion mode, R^2Y=0.974 and Q^2Y=0.953. As shown in Fig. S3, the R^2Y and Q^2Y values of the data indicated that the models had high goodness-of-fit and predictive ability.

Subsequently, screening was conducted based on the VIP value, P-value and FC of each m/z signal. After SCI, 113 differential data points were observed in the ventral horn with VIP values >1 and P<0.05, 96 of which were in the positive mode and 17 of which were in the negative mode. The dorsal horn had 107 differential data points with VIP values >1 and

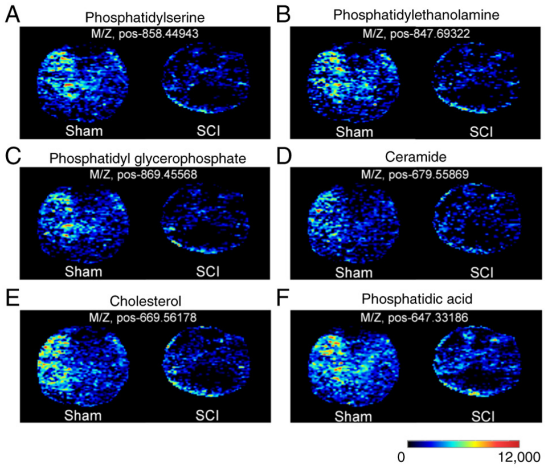

Figure 3. M/Z signal intensity imaging of representative lipid metabolites. The color scale, ranging from blue to red, represents the intensity gradient from low to high. (A) Phosphatidylserine, (B) phosphatidylethanolamine, (C) phosphatidyl glycerophosphate, (D) ceramide, (E) cholesterol and (F) phosphatidic acid showed various alterations after SCI in different anatomical structures. SCI, spinal cord injury; M/Z, mass-to-charge ratio; pos, positive ion mode.

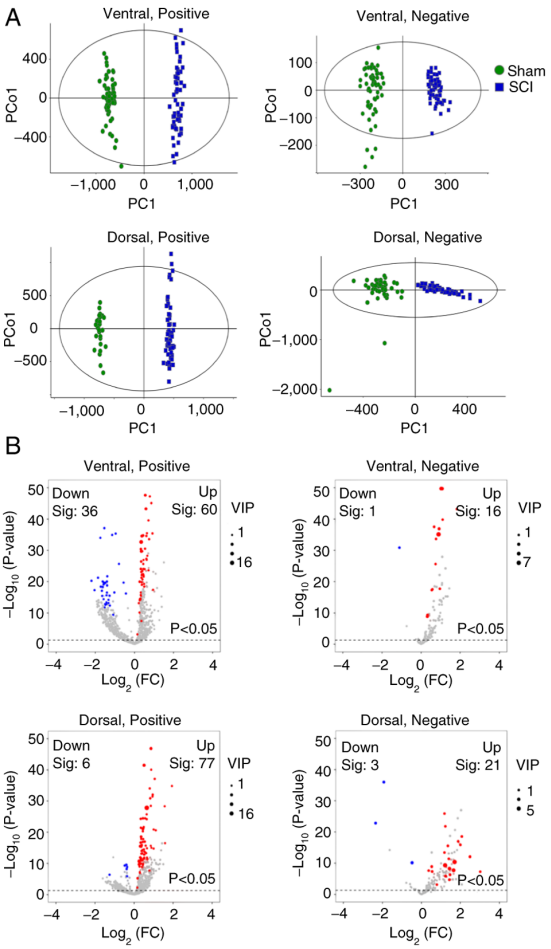

Figure 4. Metabolite alterations in ventral and dorsal horns following SCI. (A) Group separation on orthogonal partial least squares-discriminant analysis scores plots. (B) Content changes of mass-to-charge ratio signals are displayed by volcano plots. Signals with VIP values >1 are marked as red dots (upregulation) and blue dots (downregulation). The horizontal dotted lines show the cut-off level of P<0.05. FC, fold change; VIP, variable importance in projection; SCI, spinal cord injury; PC1, principal component 1; PoC1, first orthogonal component; Sig, significant.

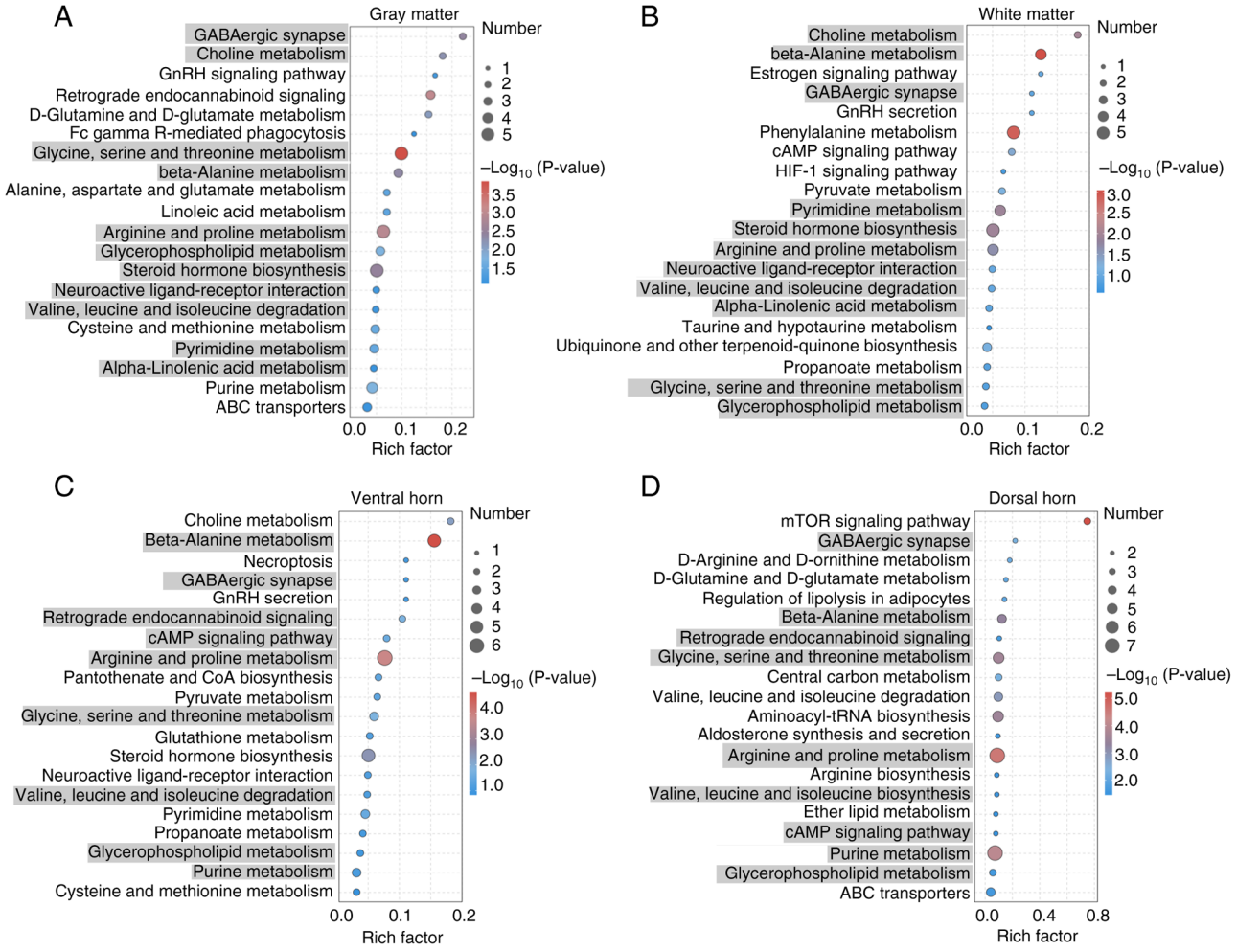

Figure 5. Functional enrichment analysis of differential metabolites. Altered metabolic terms in the (A) gray and (B) white matter following SCI. Altered metabolic terms in the (C) ventral and (D) dorsal horns following SCI. Terms that are enriched in both the gray and white matter, as well as in the ventral and dorsal horns, are marked with gray shading. The color code from blue to red indicates the sequential decrease of the P-value, while the dot size indicates the number of metabolites enriched in each pathway. SCI, spinal cord injury.

P<0.05, 83 of which were in the positive mode and 24 of which were in the negative mode (Fig. 4B). Further analysis of these annotated m/z signals revealed 315 differential metabolites in the ventral horn and 258 differential metabolites in the dorsal horn after SCI (Table SIII). A total of 134 metabolites increased in both the ventral and dorsal horns, whereas 10 metabolites decreased in both the ventral and dorsal horns. Similar to the gray and white matter, the number of metabolites was increased after injury in both the ventral and dorsal horns. The decreased metabolites contain large amounts of lipids. For example, PS, PA and PGP were mainly decreased in the ventral horn, whereas PE was mainly decreased in the dorsal horn (Table SIV). The raw m/z signal intensity images are also presented in Fig. 3.

Functional enrichment analysis of differential metabolites. Next, functional enrichment analysis of these differential metabolites was performed, with the top 20 terms shown in Fig. 4. The Y-axis represents the functional terms, and the X-axis represents the Rich factor (number of significantly different metabolites/number of total metabolites in the term). The larger the Rich factor, the greater the degree of enrichment. The color code from blue to red indicates the sequential decrease of the P-value, while the dot size indicates the number of metabolites. The larger the dot, the greater the number of metabolites enriched in the pathway.

The analysis revealed that certain terms were specific to one anatomical structure, while others were common to both. For example, 'ABC transporters', 'purine metabolism' and 'cysteine and methionine metabolism' were exclusively enriched in gray matter, whereas 'propanoate metabolism', 'ubiquinone and other terpenoid-quinone biosynthesis' and 'taurine and hypotaurine metabolism' were uniquely enriched in the white matter. Several amino acid metabolism terms, such as 'glycine, serine and threonine metabolism', 'arginine and proline metabolism' and 'beta-alanine metabolism', were enriched in both the gray and white matter. In these terms, inosine, which is involved in 'purine metabolism', was upregulated in the gray matter, while lactic acid, which is involved in 'propanoate metabolism', was upregulated in the white matter. Additionally, spermidine, which contributes to 'arginine and proline metabolism', was upregulated in both the gray and white matter (Fig. 5A and B). 'Cysteine and methionine metabolism', 'glutathione metabolism' and 'neuroactive ligand-receptor interaction' were exclusively enriched in the ventral horn, whereas 'ether lipid metabolism',

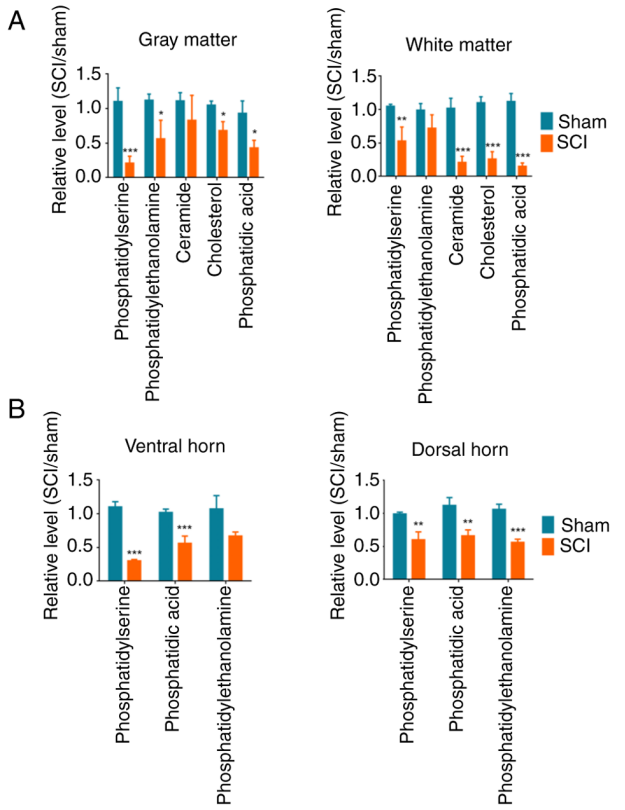

Figure 6. Confirmation of the representative metabolite changes after spinal cord injury. (A) Metabolite changes in the gray and white matter. (B) Metabolite changes in the ventral and dorsal horns. *P<0.05, **P<0.01 and ***P<0.001 vs. sham. SCI, spinal cord injury.

'aldosterone synthesis and secretion' and 'aminoacyl-tRNA biosynthesis' were uniquely enriched in the dorsal horn. Several terms, such as 'retrograde endocannabinoid signaling' and 'purine metabolism' were enriched in both the ventral and dorsal horns. In these terms, glutamine, which is involved in 'glutathione metabolism', was upregulated in the gray matter, while arginine, leucine and isoleucine, which are involved in 'aminoacyl-tRNA biosynthesis', were upregulated in the dorsal horn. Additionally, inosine, which contributes to 'purine metabolism', was upregulated in both the ventral and dorsal horns (Fig. 5C and D). These metabolites play crucial roles in SCI, and their implications are further discussed below.

Verification of the mass spectrometry results. As aforementioned, numerous lipid metabolites were reduced after SCI. Typical lipid metabolites were selected for ELISA quantitative analysis, which confirmed the observed changes by metabolomics. Among these, PS was significantly decreased in the gray matter, whereas CE and Cer were significantly decreased in the white matter in the SCI group compared with those in the sham group. PA exhibited significant differences in both the gray and white matter. In addition, PS was significantly decreased in the ventral horn, whereas PE was significantly decreased in the dorsal horn in the SCI group compared with those in the sham group (Fig. 6). These results indicated that different metabolite changes were observed among the gray and white matter, and the ventral and dorsal horns after SCI.

Discussion

Bulk metabolomics requires homogenization of the sample and is thus unable to discern metabolic differences at the cellular or tissue level (11,16,17). A recent study attempted to explore the metabolic changes on single-cell resolution (18). The spinal cord contains mainly neuronal white matter tracts and gray matter cell bodies. A transverse section reveals a distinct 'butterfly' pattern of gray matter surrounded by white matter (6). This indicates that bulk metabolomics is not suitable for analyzing metabolite differences between the white matter and the gray matter after SCI. Spatial metabolomics can directly obtain the content and spatial distribution of known or unknown metabolites in specific anatomical tissues or organs, such as the spinal cord. Spatial metabolomics has been used to evaluate liver diseases, kidney repair, cancer and cerebral ischemia (19-22).

The primary stage of SCI, occurring 0-14 days post-injury, is also considered the acute phase that begins immediately following traumatic injury. The present study employed a spinal cord transection model and spatial metabolomics to reveal the metabolic profiles of the gray and white matter on the seventh day post-injury. While the current findings provide valuable insights, incorporating data from multiple time points would enhance the depth of understanding of the metabolic changes. The lack of temporal data represents an important limitation, as it constrains the ability to comprehensively assess the progression and temporal dynamics of metabolic changes following SCI. Metabolite levels in spinal cord are expected to vary substantially across different stages of injury, spanning the acute, subacute and chronic phases. For example, glutamate levels were transiently elevated during the acute phase, while a gradual decline in N-acetyl aspartate was often observed in the chronic phase (23,24). By focusing on a single time point, critical fluctuations or patterns that could elucidate the mechanisms underlying injury progression and recovery may have been overlooked in the present study. Additionally, prior studies suggest that following spinal cord transection, animals exhibit slight motor function recovery at ~14 days post-injury, although the precise mechanisms driving this recovery remain unclear (2,5,25). This is considered to be a distinct area for further investigation. Future studies should adopt a longitudinal design, incorporating multiple sampling points throughout the injury timeline. This approach would enable a more comprehensive analysis of the dynamic interplay between metabolic changes and physiological processes, offering a holistic understanding of SCI pathology and recovery. Such data could also refine therapeutic windows and guide the development of personalized treatment strategies tailored to the temporal profile of metabolic alterations.

The results of the present study demonstrated that the metabolite profiles of the white and gray matter, as well as those of the ventral and dorsal horns, differ following SCI. A substantial portion of the decreased metabolites were lipids, which attracted our attention. PS and PE mainly decreased in the gray matter, CE and Cer mainly decreased in the white matter, and PA decreased in both the gray and white matter. PS is a phospholipid component of the cell membrane that is abundant in the central nervous system. During apoptosis, PS is exposed on the outer leaflet of the plasma membrane, while under normal

conditions, PS restricted to the inner leaflet regulates signaling pathways such as the protein kinase C and PI3K/AKT pathways (26). It has been shown that PS exerts anti-inflammatory effects on the central nervous system. PS has been indicated to inhibit the pro-inflammatory cytokines TNF-α and IL-1β induced by lipopolysaccharide, and promote the production of the anti-inflammatory cytokines TGF-β and prostaglandin E2 in microglia (27). In ischemia/reperfusion injury of the spinal cord, PS levels decreased during ischemia and were only partially restored after long-term reperfusion (28). These findings indicate that if PS levels in the gray matter can be upregulated, it may promote the survival of neurons after SCI.

PE is synthesized from cytidine, ethanolamine, diphosphate and diglycerides. In mammals, PE is found particularly in the nervous tissue, where it constitutes 45% of all phospholipids (29). The results of the present study revealed a decrease in PE levels in the gray matter, particularly in the dorsal horn. Spinal cord ischemia has been indicated to cause notable degradation of PE in the dorsal horns (28). PE has a marked anti-inflammatory effect, particularly on oxidized low-density lipoprotein-induced macrophage inflammation. Cellular PE levels were significantly decreased in response to oxidized low-density lipoprotein induction, while exogenous PE could alleviate inflammation in oxidized low-density lipoprotein-stimulated cells (30). In a previous study, treatment with phosphatidylethanolamine-binding protein 1 decreased oxidative stress and inflammation, improving neuronal survival after spinal cord ischemia (31). Therefore, decreased PE in the gray matter may contribute to neuroinflammatory and oxidative damage after SCI.

CE and Cer levels were significantly reduced in the white matter after SCI. CE is widely distributed in body tissues, particularly in the brain and spinal cord. It is not only the basic structural component of cell membranes, but also a precursor of several lipid metabolites, such as steroids, hormones and bile acids (32). Although some patients with SCI have reduced blood CE levels, there is no evidence that CE can alleviate or worsen SCI (33). The current opinion is that CE is not directly involved in inflammatory responses, as CE is not among the inflammatory proteins produced by the immune system. However, evidence shows that CE accumulation in immune cells promotes inflammatory responses, such as the activation of toll-like receptor signaling and inflammasomes (32). Cer is another important metabolite composed of sphingosine and fatty acids connected by amide bonds and is present in large amounts in the cell membrane (34). Researchers have demonstrated that exogenous Cer promotes the survival or death of spinal motor neurons by regulating apoptosis in a dose-dependent manner. Inhibition of Cer biosynthesis improved motor function and reduced neutrophil infiltration and cytokine production in an animal model of SCI (35). Therefore, decreased CE levels in the spinal cord may have no obvious physiological or pathological significance. Cer may have bidirectional regulatory effects on the spinal cord via complex underlying mechanisms.

In addition to lipids, numerous other metabolites were significantly altered and may play important roles in SCI. Inosine levels were elevated in the gray matter. Inosine is a purine nucleoside in which hypoxanthine is attached to ribofuranose via a β-N (9)-glycosidic bond. Inosine has been shown to enhance axon sprouting and motor recovery, as well as reduce secondary degeneration and cell death in adult SCI rats (25,36). Hu *et al* (37) reported that overall lactate levels are increased in the spinal cord to promote microglial scar formation following SCI. The present study also identified a specific elevation of lactic acid in the white matter. Additionally, it was observed that spermidine was upregulated in both the gray and white matter. Spermidine has been demonstrated to have protective effects against neurotrauma (38). In our previous studies, eukaryotic translation initiation factor 5A, which is hypusinated by spermidine, was not only shown to enhance neuromuscular junction connectivity but also promote synaptic plasticity in SCI rats (2,5). These findings suggest that spermidine may play a role in promoting spinal cord repair following injury.

Amino acids presented significant metabolic changes after SCI in both the gray and white matter. Several studies have focused on changes in amino acid levels in the spinal cord. High-performance liquid chromatography results showed that glutamate and aspartate levels decreased after SCI (39). Arginine is a semi-essential amino acid involved in neuronal cell survival and functionality. After SCI, arginine was demonstrated to enhance the inflammatory response, thereby exacerbating secondary injuries (40). Injury causes the spinal cord to release neurotoxic amino acids, particularly glutamate. It has been shown that the concentration of amino acids increases locally after injury and decreases with increasing distance from the center of the injury. A number of glutamate receptors are present on the cell membrane. When glutamate released by injury binds to its receptors, the membrane potential changes, thereby damaging the cells. Therefore, modifying the activity of glutamate receptors on the cell membrane using glutamate release inhibitors can result in antioxidant, nourishing and neuroprotective effects (41).

In conclusion, the present study demonstrated that the metabolic profiles of the gray matter, white matter, dorsal horn and ventral horn following SCI were different. Altered metabolites may be important in the pathogenesis of secondary SCI and may consequently represent potential therapeutic targets for treatment.

Acknowledgements

The authors would like to thank Shanghai Luming Biotechnology Co., Ltd., for performing the metabolomics data analysis.

Funding

The present study was supported by the National Natural Science Foundation of China (grant nos. 82271354 and 82001269) and the Natural Science Foundation of Chongqing (grant no. CSTB2023NSCQ-MSX0717).

Availability of data and materials

The metabolomics data generated in the present study may be found in Proteomics Identification Database under accession no. PXD060179 or at the URL: https://www.ebi.ac.uk/pride/archive/projects/PXD060179. The other data

generated in the present study may be requested from the corresponding author.

Authors' contributions

FFS designed the study. CL and YT performed the experiments. CL and FFS analyzed the data. CL and FFS confirm the authenticity of all the raw data, and wrote the manuscript. All authors read and approved the final manuscript.

Ethics approval and consent to participate

The animal experiments were approved by the Chongqing Medical University Ethics Committee on Animal Research (Chongqing, China; approval no. 2022-0115).

Patient consent for publication

Not applicable.

Competing interests

The authors declare that they have no competing interests.

References

1. GBD Spinal Cord Injuries Collaborators: Global, regional, and national burden of spinal cord injury, 1990-2019: A systematic analysis for the Global Burden of Disease Study 2019. Lancet Neurol 22: 1026-1047, 2023.
2. Shang FF, Zhao W, Zhao Q, Liu J, Li DW, Zhang H, Zhou XF, Li CY and Wang TH: Upregulation of eIF-5A1 in the paralyzed muscle after spinal cord transection associates with spontaneous hindlimb locomotor recovery in rats by upregulation of the ErbB, MAPK and neurotrophin signal pathways. J Proteomics 91: 188-199, 2013.
3. Liu W, Shang FF, Xu Y, Belegu V, Xia L, Zhao W, Liu R, Wang W, Liu J, Li CY and Wang TH: eIF5A1/RhoGDIα pathway: A novel therapeutic target for treatment of spinal cord injury identified by a proteomics approach. Sci Rep 5: 16911, 2015.
4. Zheng Q, Lin R, Wang D, Zheng C and Xu W: Effects of circulating inflammatory proteins on spinal degenerative diseases: Evidence from genetic correlations and Mendelian randomization study. JOR Spine 7: e1346, 2024.
5. Shang FF, Xia QJ, Liu W, Xia L, Qian BJ, You L, He M, Yang JL and Wang TH: miR-434-3p and DNA hypomethylation co-regulate eIF5A1 to increase AChRs and to improve plasticity in SCT rat skeletal muscle. Sci Rep 6: 22884, 2016.
6. Varma AK, Das A, Wallace G IV, Barry J, Vertegel AA, Ray SK and Banik NL: Spinal cord injury: A review of current therapy, future treatments, and basic science frontiers. Neurochem Res 38: 895-905, 2013.
7. Fujieda Y, Ueno S, Ogino R, Kuroda M, Jönsson TJ, Guo L, Bamba T and Fukusaki E: Metabolite profiles correlate closely with neurobehavioral function in experimental spinal cord injury in rats. PLoS One 7: e43152, 2012.
8. Peng J, Zeng J, Cai B, Yang H, Cohen MJ, Chen W, Sun MW, Lu CD and Jiang H: Establishment of quantitative severity evaluation model for spinal cord injury by metabolomic fingerprinting. PLoS One 9: e93736, 2014.
9. Baker SA and Rutter J: Metabolites as signalling molecules. Nat Rev Mol Cell Biol 24: 355-374, 2023.
10. Gorgey AS, Dolbow DR, Dolbow JD, Khalil RK, Castillo C and Gater DR: Effects of spinal cord injury on body composition and metabolic profile - part I. J Spinal Cord Med 37: 693-702, 2014.
11. Alexandrov T: Spatial metabolomics: From a niche field towards a driver of innovation. Nat Metab 5: 1443-1445, 2023.
12. Arifin WN and Zahiruddin WM: Sample size calculation in animal studies using resource equation approach. Malays J Med Sci 24: 101-105, 2017.
13. Scheff SW, Saucier DA and Cain ME: A statistical method for analyzing rating scale data: The BBB locomotor score. J Neurotrauma 19: 1251-1260, 2002.
14. Bemis KA, Föll MC, Guo D, Lakkimsetty SS and Vitek O: Cardinal v. 3: A versatile open-source software for mass spectrometry imaging analysis. Nat Methods 20: 1883-1886, 2023.
15. Triba MN, Le Moyec L, Amathieu R, Goossens C, Bouchemal N, Nahon P, Rutledge DN and Savarin P: PLS/OPLS models in metabolomics: The impact of permutation of dataset rows on the K-fold cross-validation quality parameters. Mol Biosyst 11: 13-19, 2015.
16. Chen X, Shu W, Zhao L and Wan J: Advanced mass spectrometric and spectroscopic methods coupled with machine learning for in vitro diagnosis. View 4: 20220038, 2023.
17. Zhang J, Hu A, Chen X, Shen F, Zhang L, Lin Y and Shen H: Pan-targeted quantification of deep and comprehensive cancer serum proteome improves cancer detection. View 4: 20220039, 2023.
18. Cao J, Yao QJ, Wu J, Chen X, Huang L, Liu W, Qian K, Wan JJ and Zhou BO: Deciphering the metabolic heterogeneity of hematopoietic stem cells with single-cell resolution. Cell Metab 36: 209-221. e6, 2024.
19. Wang H, Li Z, Cao G, Tang L, Zhou R, Li C, Zhang J, Wu H, Li X and Yang H: Targeted energy metabolomics combined with spatial metabolomics study on the efficacy of guhong injection against cerebral ischemia reperfusion. Mol Neurobiol 60: 5533-5547, 2023.
20. Santos AA, Delgado TC, Marques V, Ramirez-Moncayo C, Alonso C, Vidal-Puig A, Hall Z, Martínez-Chantar ML and Rodrigues CMP: Spatial metabolomics and its application in the liver. Hepatology 79: 1158-1179, 2024.
21. Young LEA, Conroy LR, Clarke HA, Hawkinson TR, Bolton KE, Sanders WC, Chang JE, Webb MB, Alilain WJ, Vander Kooi CW, *et al*: In situ mass spectrometry imaging reveals heterogeneous glycogen stores in human normal and cancerous tissues. EMBO Mol Med 14: e16029, 2022.
22. Zheng Q, Wang D, Lin R, Li Z, Chen Y, Chen R, Zheng C and Xu W: Effects of circulating inflammatory proteins on osteoporosis and fractures: Evidence from genetic correlation and Mendelian randomization study. Front Endocrinol (Lausanne) 15: 1386556, 2024.
23. Afjehi-Sadat L, Brejnikow M, Kang SU, Vishwanath V, Walder N, Herkner K, Redl H and Lubec G: Differential protein levels and post-translational modifications in spinal cord injury of the rat. J Proteome Res 9: 1591-1597, 2010.
24. Di Giulio F, Castellini C, Palazzi S, Tienforti D, Antolini F, Felzani G, Baroni MG and Barbonetti A: Correlates of metabolic syndrome in people with chronic spinal cord injury. J Endocrinol Invest 47: 2097-2105, 2024.
25. Kim D, Zai L, Liang P, Schaffling C, Ahlborn D and Benowitz LI: Inosine enhances axon sprouting and motor recovery after spinal cord injury. PLoS One 8: e81948, 2013.
26. Ma X, Li X, Wang W, Zhang M, Yang B and Miao Z: Phosphatidylserine, inflammation, and central nervous system diseases. Front Aging Neurosci 14: 975176, 2022.
27. De SR, Ajmone-Cat MA, Nicolini A and Minghetti L: Expression of phosphatidylserine receptor and down-regulation of pro-inflammatory molecule production by its natural ligand in rat microglial cultures. J Neuropathol Exp Neurol 61: 237-244, 2002.
28. Lukacova N, Halát G, Chavko M and Marsala J: Ischemia-reperfusion injury in the spinal cord of rabbits strongly enhances lipid peroxidation and modifies phospholipid profiles. Neurochem Res 21: 869-873, 1996.
29. Vance JE and Tasseva G: Formation and function of phosphatidylserine and phosphatidylethanolamine in mammalian cells. Biochim Biophys Acta 1831: 543-554, 2013.
30. Hao T, Fang W, Xu D, Chen Q, Liu Q, Cui K, Cao X, Li Y, Mai K and Ai Q: Phosphatidylethanolamine alleviates OX-LDL-induced macrophage inflammation by upregulating autophagy and inhibiting NLRP1 inflammasome activation. Free Radic Biol Med 208: 402-417, 2023.
31. Kim W, Cho SB, Jung HY, Yoo DY, Oh JK, Choi GM, Cho TG, Kim DW, Hwang IK, Choi SY and Moon SM: Phosphatidylethanolamine-binding protein 1 ameliorates ischemia-induced inflammation and neuronal damage in the rabbit spinal cord. Cells 8: 1370, 2019.
32. Tall AR and Yvan-Charvet L: Cholesterol, inflammation and innate immunity. Nat Rev Immunol 15: 104-116, 2015.

33. Syed MUS, Khan Z, Zulfiqar A, Basham MA, Abdul Haseeb H, Azizullah S, Ismail H, Elbahnasawy M, Nadeem Z and Karimi S: Electrocardiographic abnormalities in patients with spinal cord injury with deranged lipid profile. Cureus 13: e18246, 2021.
34. Arana L, Gangoiti P, Ouro A, Trueba M and Gómez-Muñoz A: Ceramide and ceramide 1-phosphate in health and disease. Lipids Health Dis 9: 15, 2010.
35. Cuzzocrea S, Deigner HP, Genovese T, Mazzon E, Esposito E, Crisafulli C, Di Paola R, Bramanti P, Matuschak G and Salvemini D: Inhibition of ceramide biosynthesis ameliorates pathological consequences of spinal cord injury. Shock 31: 634-644, 2009.
36. Liu F, You SW, Yao LP, Liu HL, Jiao XY, Shi M, Zhao QB and Ju G: Secondary degeneration reduced by inosine after spinal cord injury in rats. Spinal Cord 44: 421-426, 2006.
37. Hu X, Huang J, Li Z, Li J, Ouyang F, Chen Z, Li Y, Zhao Y, Wang J, Yu S, *et al*: Lactate promotes microglial scar formation and facilitates locomotor function recovery by enhancing histone H4 lysine 12 lactylation after spinal cord injury. J Neuroinflammation 21: 193, 2024.
38. Huang J, Zhang H, Zhang J, Yu H, Lin Z and Cai Y: Spermidine exhibits protective effects against traumatic brain injury. Cell Mol Neurobiol 40: 927-937, 2020.
39. Watanabe M, Fujimura Y, Nakamura M, Yato Y, Ohta K, Okai H and Ogawa Y: Changes of amino acid levels and aspartate distribution in the cervical spinal cord after traumatic spinal cord injury. J Neurotrauma 15: 285-293, 1998.
40. Erens C, Van Broeckhoven J, Bronckaers A, Lemmens S and Hendrix S: The dark side of an essential amino acid: L-Arginine in spinal cord injury. J Neurotrauma 40: 820-832, 2023.
41. Liu X, Zhang Y, Wang Y and Qian T: Inflammatory response to spinal cord injury and its treatment. World Neurosurg 155: 19-31, 2021.